Synthesis of self-healing NiAl-Al2O3 composite coatings by electrochemical way

R. Troncy, L. Boccaccini, G. Bonnet, X. Montero, M.C. Galetz, F. Pedraza

Synthesis of self-healing NiAl-Al_2O_3 composite coatings by electrochemical way

R. Troncy[1, a], L. Boccaccini[1, b], G. Bonnet[1, c], X. Montero[2], M.C. Galetz[2], F. Pedraza[1, d]

[1] LaSIE, La Rochelle Université, UMR CNRS 7356, Avenue Michel Crépeau, 17042 La Rochelle Cedex 1, France

[2] DECHEMA-Forschungsinstitut, Theodor-Heuss-Allee 25, 60486 Frankfurt, Germany

[a]romain.troncy1@univ-lr.fr, [b]louis.boccaccini@univ-lr.fr, [c]gbonnet@univ-lr.fr, [d]fpedraza@univ-lr.fr

Abstract

Nickel aluminide diffusion coatings act like an aluminium reservoir to form protective alumina scales at high temperatures. However, interdiffusion phenomena play a critical role in the metallurgical integrity of these coatings. This work explores a new type of self-healing coating for high temperature oxidation applications. Micro-reservoirs consisting of an aluminium-rich intermetallic core (Al_3Ni_2) and an aluminium oxide shell are embedded in a nickel aluminide matrix (NiAl). This new type of coating has been synthesized by an electrochemical chemical route to trap the micro-reservoirs in an electrodeposited nickel matrix followed by aluminization via a slurry route. Under high temperature oxidation conditions, the micro-reservoirs allow to form a diffusion barrier and to release Al into the coating matrix. These two simultaneous phenomena make it possible to maintain a sufficient amount of aluminium and ensure the unique formation of α-alumina at the surface of the coatings, hence to possibly increase the lifespan of the aluminium diffusion coatings.

Keywords: Composite coating; NiAl-Al_2O_3; Electrodeposition; Self-healing coating; Oxidation

1. Introduction

One of the effective and economical ways to protect materials against oxidation and corrosion is to use coatings. The nature of the coatings depends on the conditions of use and the materials to be protected. In recent years, various studies have focused on the synthesis of self-healing, self-regenerating or intelligent coatings [1-3]. These coatings have the ability to repair physical damage to the coatings and regain their protective functions (without or with minimal human intervention).

One of the first and best-known self-healing properties were applied on polymer coatings [1]. Two types of microreservoirs are trapped in the coating and upon physical damage (e.g. scratches, cracks, etc.), the microreservoirs break and release their content (building blocks and catalysts) and polymerize in the defect to seal it, thus preventing corrosion of the substrate. [1-2]. Based on a similar approach, self-healing ceramic YSZ thermal barrier coatings were synthetized for high temperature applications whereby the micro-reservoirs are made of $MoSi_2$(Al,B). [2]. Upon initiation and propagation of a crack, the oxidation of the healing agent forms liquid SiO_2 that flows into the crack. SiO_2 also reacts with the Zr of the coating to form solid $ZrSiO_4$ and thus block the propagation of the crack [2]. Such self-healing coatings use a liquid phase, which is undesirable for all types of coatings, especially for β-NiAl coatings used for protection against high temperature oxidation since Ni can dissolve in molten Al [3].

Therefore, the present investigation precisely focuses in the synthesis of self-healing, which are typically synthetized by chemical-vapor deposition or slurry-aluminizing [4-9]. Upon oxidation, these aluminium-rich coatings allow the formation of a dense, uniform and slow-growing Al_2O_3 layer [4-5, 10-11]. However, the difference in aluminium concentration between the coating and the substrate induces significant interdiffusion between the coating and the substrate. Below a certain aluminium threshold, which essentially depends on the composition of the material, the temperature of the tests and the

partial pressure of oxygen, non-protective Ti, Ta, and Ni oxides can form and induce a significant mass variation through fast oxidation kinetics [12].

In this context, our previous works investigated the use of aluminothermic reactions to fabricate self-regenerating coatings [13-14]. Yet, an interfacial NiO oxide layer formed between the coating and the Ni substrate and the results on interdiffusion were not assessed. On the contrary, this work studies composite coatings consisting of a β-NiAl intermetallic matrix and pre-oxidized Al_3Ni_2 micro-reservoirs to increase the life of the coatings for high temperature oxidation applications. To achieve this, Al_3Ni_2 particles were first synthesized and oxidized to form a thin scale of Al_2O_3. They were then incorporated in a nickel electrodeposited matrix and finally aluminized by slurry. Adding Al_3Ni_2 particles has two advantages. First, the addition of particles provides barriers to limit the diffusion of aluminium into the substrate and of nickel into the coating. Secondly, whenever the difference in aluminium concentration between the coating and the particles is sufficiently large, the aluminium contained in the particles should gradually diffuse into the coating matrix. The goal is to maintain an aluminium threshold for a longer time, thus delaying the appearance of non-protective oxides and thus increasing the lifetime of the material. This approach has never been reported before in Al diffusion coatings.

In summary, this study focuses on the manufacturing, microstructure of such self-healing coatings and their oxidation behaviour. For this, various parameters such as current density, aluminizing temperature and time were investigated.

2. Experimental procedure

Various coatings were synthesized in several steps and using different coating techniques to evaluate the self-healing character of the β-NiAl coatings on pure (99.98 wt.%, Goodfellow) Ni samples (Table I). The substrateswere cut from 12.7 mm diameter cylindrical rods into coupons of about 1.5 mm thickness, polished with SiC P180 papers and then rinsed with deionized water and cleaned in ethanol. After the surface preparation, Ni electroplated layers with and without preoxidized Al_3Ni_2 micro-containers followed by slurry aluminizing were produced. Comparison with simple slurry aluminized coatings, i.e. no intermediate electroplated was also conducted. After aluminizing, the coating surfaces were sandblasted (Al_2O_3) to remove the typical residue (bisque) of the slurry coatings. The description of each method is given in the following paragraphs.

Table I.- Summary of the different coating strategies to evaluate the self-healing character of the β -NiAl coatings.

Denomination	**Coating process**			
Ni plating	--	Electro-deposition (without $Al_3Ni_{2(ox)}$)	sandblasting	aluminizing
Electro-codeposition WITH Ni flash	Ni "flash"	Electro-codeposition (WITH $Al_3Ni_{2(ox)}$)		
Electro-codeposition WITHOUT Ni flash	--	Electro-codeposition (WITHOUT $Al_3Ni_{2(ox)}$)		
Ni substrate	--	--	--	

2.1. Synthesis and pre-oxidation of Al_3Ni_2 microparticles

Al_3Ni_2 microsized reservoirs were synthetized by various steps including pack aluminizing, grinding, milling and sieving and final preoxidation. For this, Ni sheets with a thickness of 250 µm and a purity of

99.98% (GoodFellow) were aluminized by pack cementation. The Ni sheets were embedded in a powder mixture made of 56 wt. % of Al_2O_3 powder, 40 wt.% of Al powder and 4 wt. % of NH_4Cl. The powders were mixed using a three-dimensional mixer (Turbula System Schatz type T2 F). The crucible was closed and heated at 800°C for 50h under Ar/5%H_2 atmosphere to obtain the Al-rich and brittle Al_3Ni_2 intermetallic phase across the foil.

These samples were then ground for 5 min at 30 Hz into powder first with a jar milling to obtain coarse particles (Retsch MM2 mixer mill). To homogenize and reduce further the particle size, a planetary ball milling (P100 - Retsch) was used. The powders previously obtained with the jar milling were placed at half of the volume of the crucible and filled with zirconia balls with a diameter of 2.15 mm. The free space between the particles was filled with 96% pure ethanol and the crucible was finally sealed. The crucible was then rotated at 500 rpm for 8 h. After the mechanical treatment, the crucible was placed in an oven at 60°C for 12 hours to evaporate the ethanol. The particles were subsequently sorted using several sieves positioned on a JEL 200 sieve machine. The sieves consisted of 5 assembly sieves made up of 630 µm, 250 µm, 160 µm, 100 µm and 25 mesh sizes. µm.

Finally, the last step consisted in the pre-oxidation of the particles to form an Al_2O_3 shell while keeping a metallic core. For this, the particles were oxidized at 1100°C for 15 min under Ar. After the 15 min, the particles were quenched in laboratory air.

After the oxidation step, the particles show an irregular morphology with an Al_3Ni_2/β-NiAl core and an aluminium oxide shell (Figure 2). The image analysis indicated a d_{50} of the pre-oxidized particles of 0.49 µm with an oxide shell thickness of about 0.06 µm.

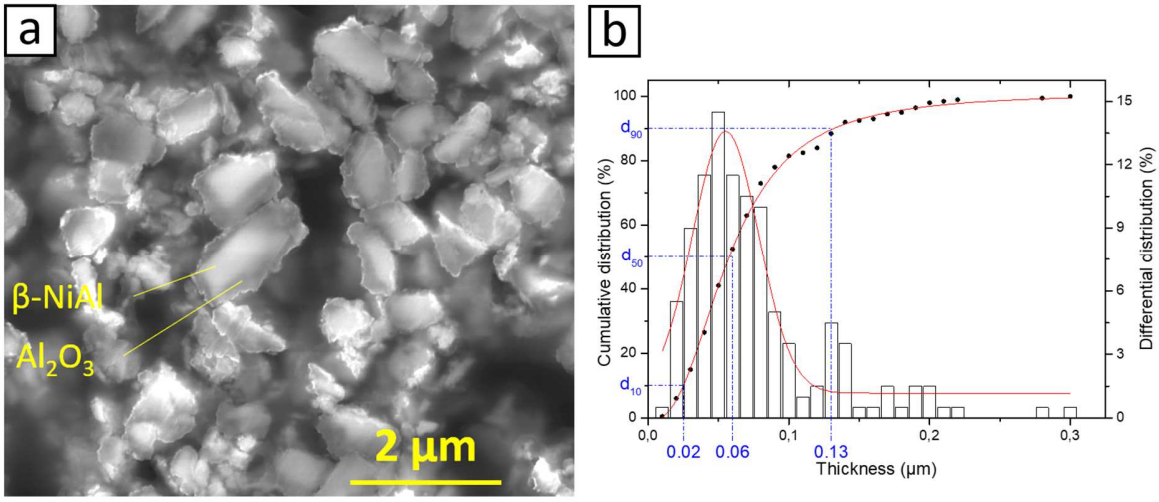

Figure 1: (a) SEM (BSE) cross-section images of the powders pre-oxidized at 1100°C for 15 min under Ar and (b) the distribution and thickness of the oxide Al_2O_3 shells.

2.2. Electro-deposition of the pure Ni and composite Ni+Al_2Ni_3(ox) layers

The polished Ni substrates were subjected to a "nickel flash" electrodeposition process in a sulfamate bath composed of 300 g/L of $Ni(SO_3NH_2)_2.4H_2O$, 30 g/L of H_3BO_3, 15 g/L of $NiCl_2.6H_2O$ and $Ni_4CO_3(OH)_6(H_2O)_4$ to adjust the pH between 4.2 and 4.3. The synthesis of a first layer of flash nickel was carried out to increase the adhesion between the composite coating and the substrate, in particular to avoid the phenomena of decohesion during the aluminization treatment. In addition, the surface of the samples being rough, the choice was made to use high current densities and significant thicknesses, namely 5 A/dm² and 10 µm (not shown). The term of "nickel flash" therefore does not appear as the most suitable and the term of "first layer" will be used subsequently. Like in the work of R. Winand, the grain microstructure of Ni electrodeposits is Basis Reproduction (B.R.) with a fine grain close to the interface and coarser grains towards the surface [15].

The samples were then cleaned and prepared for the electro-codeposition step, which will form a composite coating composed of pre-oxidized Al_3Ni_2 particles embedded in a nickel matrix. For this, the Ni-$Al_3Ni_{2(ox)}$ alloy material was prepared by the (direct current) DC electro-codeposition method on the Ni first layer with a sulfamate bath where 20 g/dm^3 of pre-oxidized particles were added. The volume percentage of trapped particles was observed (not shown) to increase from 10 to 17.5 % with increasing the current density between 2 and 5 A/dm^2 and then stabilized at 22 % for a current density of 20 A/dm² in the nickel sulfamate bath at 50°C. Therefore, the composite electroplates were fabricated with such high current density.

2.3. Aluminizing process

After the electrochemical steps, the composite Ni-$Al_3Ni_{2(ox)}$ layers were sandblasted with Al_2O_3 powders at 0.5 bar of pressure. This step is necessary to remove the pre-oxidized particles on the surface and allow the homogeneous aluminizing of the coating. Then, an Al-based slurry was sprayed on the coupons. The slurry formulation is based on a 1/10 PolyVinyl Alcohol (PVA)/deionized water solution to which 45 wt. % of spherical Al powders (4±3 µm, Hermillon Poudres, France) were added [16]. After blending, the slurries were deposited by airbrush on the Ni-$Al_3Ni_{2(ox)}$ composite layer. After each deposit, the samples were systematically dried in a stove at 50 °C for 30 min. The samples were weighed before and after slurry deposition with a 10^{-4}g precision balance to control the deposited slurry quantity.

The dry coatings were then annealed in a TGA apparatus to form the diffusion coating, under a flow of argon (20 mL/min) to prevent any significant oxidation of the substrate and of the Al particles [9]. The aluminizing treatments were carried out at different temperatures and for different times. The temperatures of 650°C and 700°C were chosen to promote Al inward diffusion while 1100°C aimed at promoting the Ni outward diffusion. Dwell times of 12h were chosen for the temperature of 650 and 700°C and of 1 min for aluminizing at 1100°C. Following these 3 different tests, the most promising heat treatments (700°C/2 h) were performed for different times (1min, 2h, 4h et 12h). In all of them, the heating and cooling rates were set at 5°C/min.

2.4. Self-healing potential of the coatings

The assessment of the self-healing potential of the synthetized coatings, various coatings were oxidized isothermally at 1000°C for 48h in synthetic air. Note that these oxidation tests were not intended to finely characterize the oxidation behaviour of the coatings but to demonstrate (or not) the self-healing nature of the coatings. Additional tests on reference aluminide coatings on raw nickel substrates and on simple nickel electrodeposit, i.e. without the incorporation of the Al_3Ni_2 microparticles were also carried

out for comparison. These two coatings were prepared by slurry aluminizing at 700°C/2h or 700°C/2h+1100°C/1min (designated thereafter as "1100°C/1min"). The nickel plating was deposited from a bath of nickel sulfamate and with a current density of 20 A/dm². Two Ni/$Al_3Ni_{2(ox)}$ composite coatings were tested, one with a first flash Ni layer over the substrate and another without the flash Ni layer. Table II summarizes the coatings that underwent the oxidation tests at 1100°C for 48h in air.

Table II: Summary table of the coatings tested in isothermal oxidation (1000°C/48h in air). All substrates are pure Ni.

First Ni layer	$Al_3Ni_{2(ox)}$+Ni	Aluminization treatment
---	---	700°C/2h
---	---	700°C/2h + 1100°C/1 min
50 µm	---	700°C/2h
50 µm	---	700°C/2h + 1100°C/1 min
10 µm	50 µm	700°C/2h
10 µm	50 µm	700°C/2h + 1100°C/1 min
---	50 µm	700°C/2h
---	50 µm	700°C/2h + 1100°C/1 min

2.5. Characterization

The characterization of the coatings was conducted with an optical microscope (LEICA DMRM microscope coupled to a LEICA MC170 HD camera) and SEM (FEI QUANTA 200F) coupled to an EDAX detector for chemical analysis, at 20 kV under low vacuum (0.9 mbar). The cross-sections were polished down to 1 µm water-based diamond suspension (Struers). Raman micro-spectrometry (Jobin Yvon LabRam HR800, λ=632.82 nm and LabRAM HR Evolution, λ=532 nm) was also carried out to identify the different oxide phases. In addition, the crystal structure was characterized by X-ray diffraction (XRD) in a Bruker AXS D8 Advance with Cu $k_{\alpha 1}$ radiation (λ=0.15406 nm).

3. Results

3.1. Influence of current density

Figure 2 shows a cross-section of the samples after electrodeposition with 20 A/dm^2. The particles embedded in the coating are evenly distributed throughout the thickness except for some clustering of particles (Figure 2.a). One shall note that the particles appear to be stable in the electrodeposition bath since the metallic core and the oxide shell are still observed (Figure 2.b). The Raman spectroscopy analysis at 632 and 532 nm allowed to unambiguously identify α-Al_2O_3 and Θ-Al_2O_3 on the shells of the particles (Figure 3). Indeed, for similar oxidation temperatures, a first layer of Θ-Al_2O_3 and a second layer of α-Al_2O_3 have been identified upon the oxidation of Al_3Ni_2 at 1100°C during 30 min [17]. In addition, the EDS spots at the core of the particles revealed about 30±4 at.% of Al. This concentration appears lower than expected compared with the theoretical value of Al_3Ni_2 (60 at.%). This result can be attributed to the fact that the volume analyzed by the EDS spots is larger than the particle size and therefore includes Ni from the matrix.

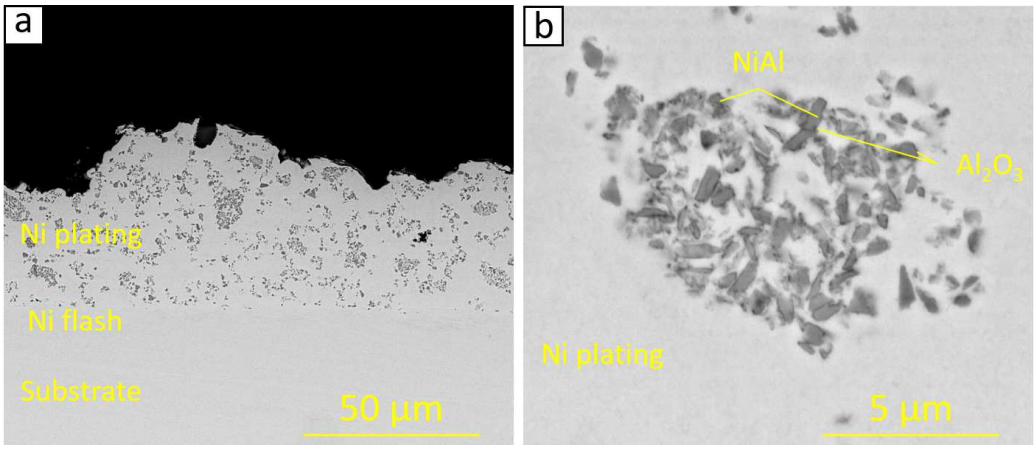

Figure 2: SEM (BSE mode) cross-sections of the composite electrodeposits with a Ni matrix and pre-oxidized Al_3Ni_2 particles.

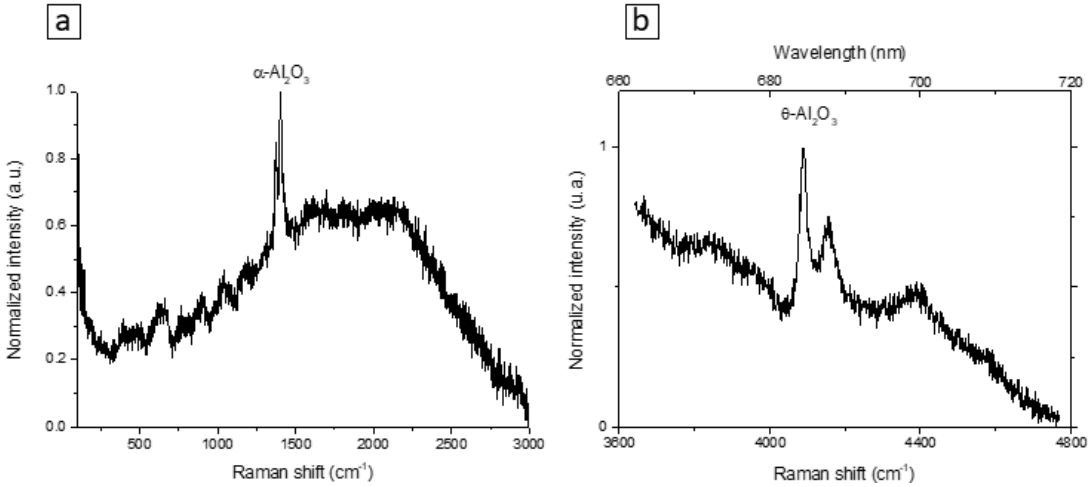

Figure 3: Raman spectra on the shells of the particles embedded in the Ni electrodeposits obtained at 20 A/dm². The spectra were collected with (a) λ=632 nm and (b) λ=532 nm lasers [18-19].

3.2. Influence of aluminizing heat treatment.

3.2.1. Influence of aluminizing temperature.

Once the electrodeposition of the composite ($Ni+Al_3Ni_{2(ox)}$) coatings was achieved, the final step consisted in aluminizing by slurry route. For this, "low" temperatures of 650 and 700°C were selected based on previous investigations conducted in our research group on Ni-based substrates [20-22]. The high-activity low temperature (HALT) aluminizing allows preferential diffusion of aluminium towards the substrate. This results in the formation of the intermetallic coating in the electroplated layer and preserves thus the structure of the coating produced by electrochemical means. In addition, a short-term aluminizing was carried out at 1100°C to achieve a low-activity high temperature (LAHT) aluminizing allowing the preferential outward diffusion of nickel [20,23].

Figure 4 shows the SEM cross-sections of the aluminized samples at 650°C/12h (Figure 4.a), 700°C/12h (Figure 4.b) and 1100°C/1min (Figure 4.c). Figure 5 gathers the diffusion profiles of aluminium in the coating (Figure 5.a) as well as the thickness of the different layers observed (Figure 5.b). For the three temperatures, the coatings obtained can be divided into four parts. The first part at the top of the coatings consists of a porous Al-rich β-NiAl intermetallic for low-temperature coatings (Figure 4.a & 4.b) and a porous Ni-rich β-NiAl intermetallic for the high-temperature treatment (Figure 4.c). In addition, inclusions of aluminium oxide can be observed in this layer. This layer appears to come from the solidification of a previous liquid phase, according to its microstructure (Figure 5.b, label "melting layer"). The thicknesses of this porous layer are 10±4 µm, 12±2 µm and 13±4 µm for the treatments of 650°C/12h, 700°C/12h, and 1100°C/1min, respectively. The second layer is the diffusion zone and shows a composite microstructure with the pre-oxidized Al_3Ni_2 particles in a matrix of β-NiAl and γ'-Ni_3Al intermetallic compounds. The intermetallic compound β-NiAl has a composition similar to the first layer, namely Al-rich β-NiAl for the aluminizing treatments at 650 and 700°C, and Ni-rich β-NiAl for the treatment of 1100°C/1min. The pre-oxidized particles appear to be homogenously distributed for the heat treatment of 650°C (Figure 4.a). For the 700°C treatment, the particles are aligned normal to the surface (Figure 4.b). For the samples aluminized at 1100°C, the particles seem to be homogeneously distributed in the first two-thirds of this layer (Figure 4.c). In the last third, no particles can be observed. In addition, the aluminium concentration is low in this part (Figure 5.a). The third interface is found between the aluminized part and the substrate with a low content of aluminium substrate. For the 650°C heat treatment (Figure 4.a), this interface consisted of an oxide. For the two other treatments, this interface is mainly made up of voids and an interfacial decohesion appears for the samples treated at 700°C/12h (Figure 4.b & 4.c). It can also be noted that oxide particles can be observed at high magnification on the upper part of the interface between the aluminized and poorly aluminized areas. The last "poorly aluminized" layer below the interface is clearly distinguished for the 650°C/12h treatment, with 10±1 µm of the electro-codeposited layer and 7±1 µm of the first layer of Ni, which have not been aluminized (Figure 4.a). For the aluminizing treatments at higher temperatures (700 and 1100°C) (Figure 4.b & 4.c), the interfaces between the electrodeposition and the first layer of Ni are less visible and it is thus difficult to differentiate these layers.

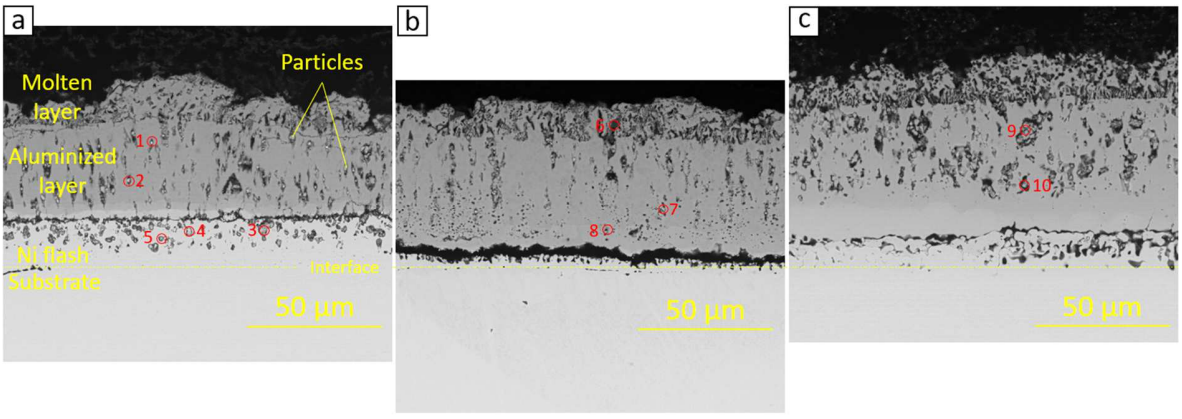

Figure 4: SEM (BSE mode) cross-section of the aluminized composite coating with a heat treatment of (a) 650°C/12h, (b) 700°C/12h and (c) 1100°C/1 min.

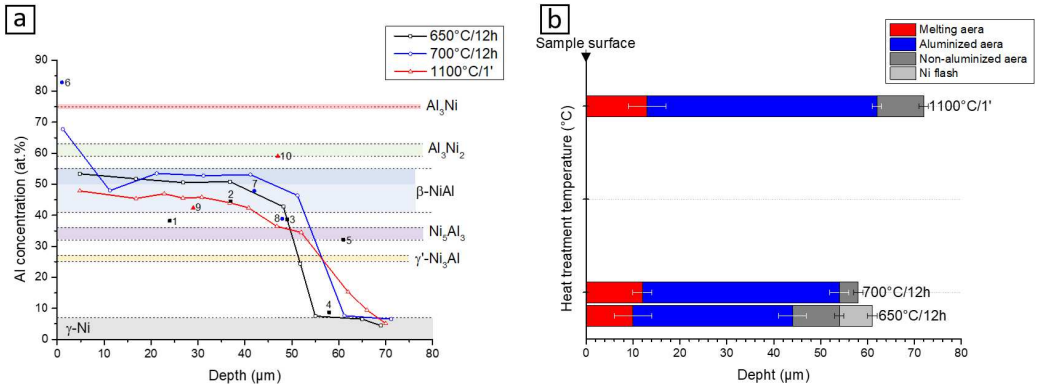

Figure 5: (a) EDS diffusion profiles made in cross-section for the different heat treatments and (b) the thickness layers of the coatings.

The Raman micro-spectroscopic analyses were carried out to identify the oxides present in the coating (Figure 6). In the non-aluminized layer (Figure 6.a & 6.d), the Θ and α-Al_2O_3 peaks can be observed for the aluminizing treatments of 650°C. For 700 and 1100°C with α-Al_2O_3 being predominant. Similar observations can be made at the interface, with the presence of Θ and α-Al_2O_3 for aluminizing treatments of 650 and 700°C (Figure 6.b & 6.e). In the aluminized layer the peaks of Θ-Al_2O_3 are clearly observed for the λ=632 nm (Figure 6.c) while the α-Al_2O_3 peaks are better highlighted with the λ= 532 nm (Figure 6.f). One shall note that the peaks of SiO_2 observed in Figure 6.c are related to the OPS polishing solution, which remained trapped in the pores present between the particles and the coating.

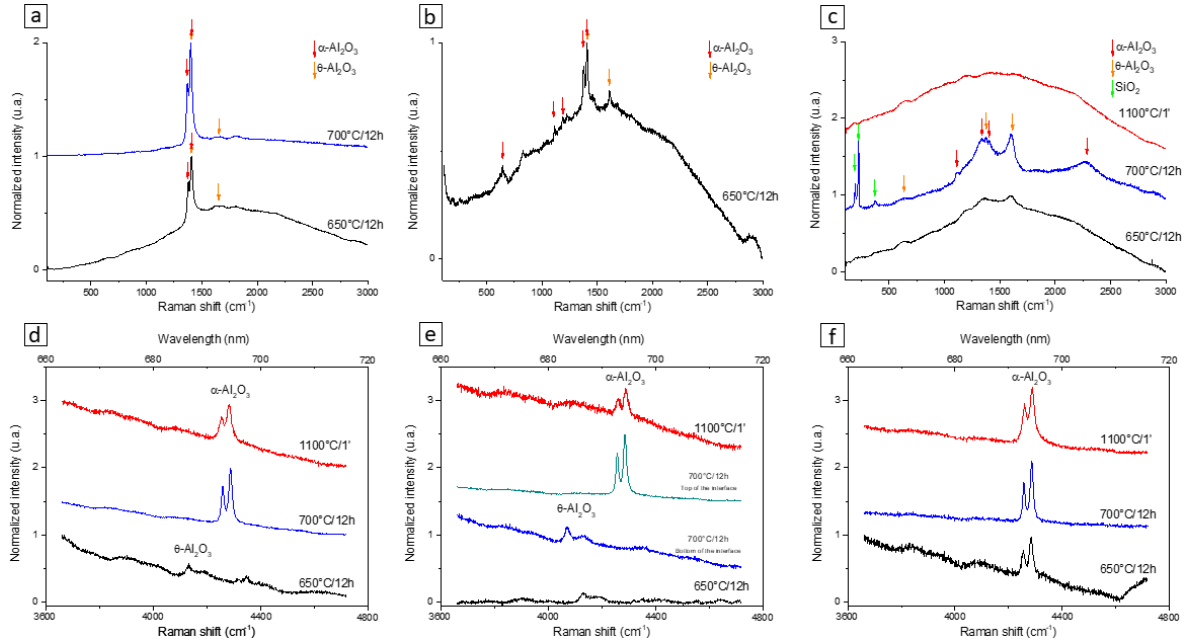

Figure 6: Raman spectra (λ=632 nm for (a), (b) and (c) and λ=532 nm for (d), (e) and (f)) on the cross-sections of the samples after the aluminization process, with (a and d) in the particles on the non-aluminized layer, (b and e) interface layer and (c and f) in the particles on the aluminized layer [18-19, 24-25].

3.2.2. Influence of aluminizing time

From the three aluminizing temperatures, 700°C was selected to investigate the influence of aluminizing time on the development of the composite coating. This choice was made because a residual thick zone of molten and oxidized aluminium remained on the surface of the coating when aluminizing at 650 and 1100°C, respectively. In addition, the amount of aluminium in the coating is uneven and dispatched in two zones (Figure 4.a & 4.c).

The microstructures of the coating after aluminizing at 700°C for 1 min, 2, 4 and 12h are shown in Figure 7. The diffusion profiles and the thicknesses of the layers are presented in Figure 10. For the heat treatments of 1 min (Figure 7.a), 2h (Figure 7.b) and 4h (Figure 7.c), the microstructure, composition and coating thickness obtained are quite similar and comparable to what was obtained at 650°C/12h (Figure 4.a). Indeed, a first porous layer due to the solidification of a liquid phase can be observed at the surface of the coating. This layer is rich in Al, with a content greater than 56 at. % of Al (Figure 8.a). The second layer consists of Al-rich β-NiAl and $Al_3Ni_{2(ox)}$ particles whose thicknesses range between 25 and 33 µm (Figure 8.b). Underneath, the non-aluminized composite electroplating is about 7±1 µm thick and the Ni flash layer over the substrate kept its thickness (10±1 µm) (Figure 8.b). It is interesting to note that the longer the aluminizing time at 700°C, the more porous becomes the interface between the aluminized and non-aluminized layers (Figure 7d).

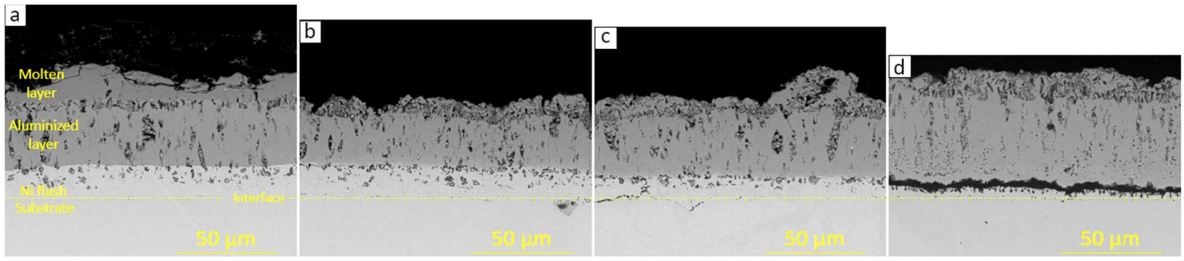

Figure 7: SEM (BSE mode) cross-section of the aluminized composite coating with a heat treatment of 700°C during (a) 1 min, (b) 2h, (c) 4h and (d) 12h.

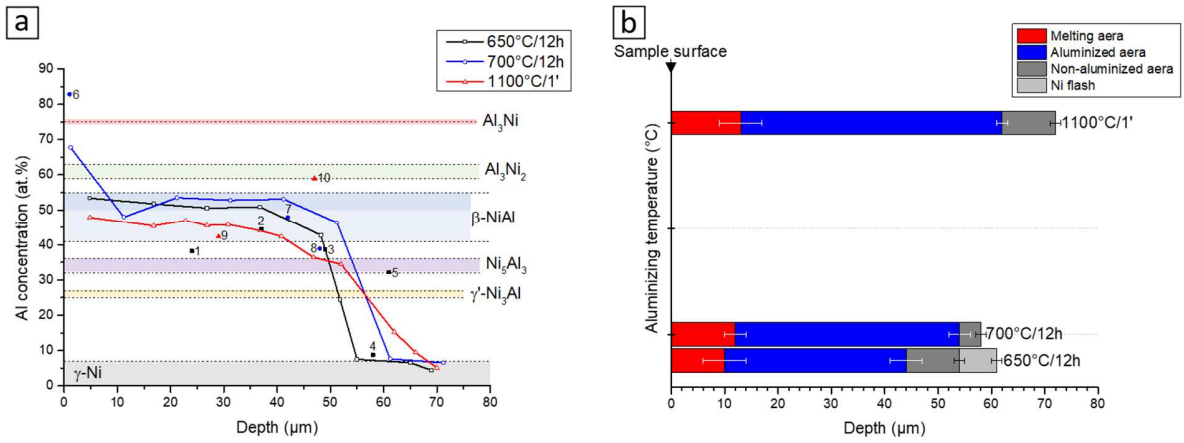

Figure 8: (a) EDS diffusion profiles made in cross-section for the different heat treatments at 700°C and (b) the thickness layers of the coatings.

The analyses of Raman spectroscopy shown in Figure 9 for the different aluminizing times indicate the formation different phases of aluminium oxide. Increasing the time in the particles of the non-aluminized layer (Figure 9.a & 9.c) increases the α-Al_2O_3 signal with the 632 nm laser (Figure 9.a). In contrast, the α-Al_2O_3 peaks are readily observed from 1 min at 700°C with the 532 nm laser (Figure 9.b). This strongly suggests that the stabilization of α-Al2O3 is only reached after 12h of exposure at 700°C. Yet, the particle/matrix interface at 700°C/12h (Figure 9.b) shows both, the Θ and α-Al2O3 polymorphs (Figure 9.d). In the particles of the aluminized layer (Figure 9.b & 9.e), Θ-Al_2O_3 appears predominant at all times although for analyses with the 532 nm laser, α-Al_2O_3 is also observed (Figure 9.e). Like with the particles of the non-aluminized layer, 12 h are required to detect the α-Al_2O_3 signal with the 632 nm laser (Figure 9.b). In addition, the traces of SiO_2 are related to the OPS polishing solution. It therefore seems that the aluminized area requires greater aluminizing time for Θ to transform into α-Al_2O_3 compared to the non-aluminized layer, that shows a majority of α-Al_2O_3 at all times. Since the annealing temperature is the same, this difference can only be attributed to the greater content of oxygen in the aluminized area according to Garriga-Majo et al. [26].

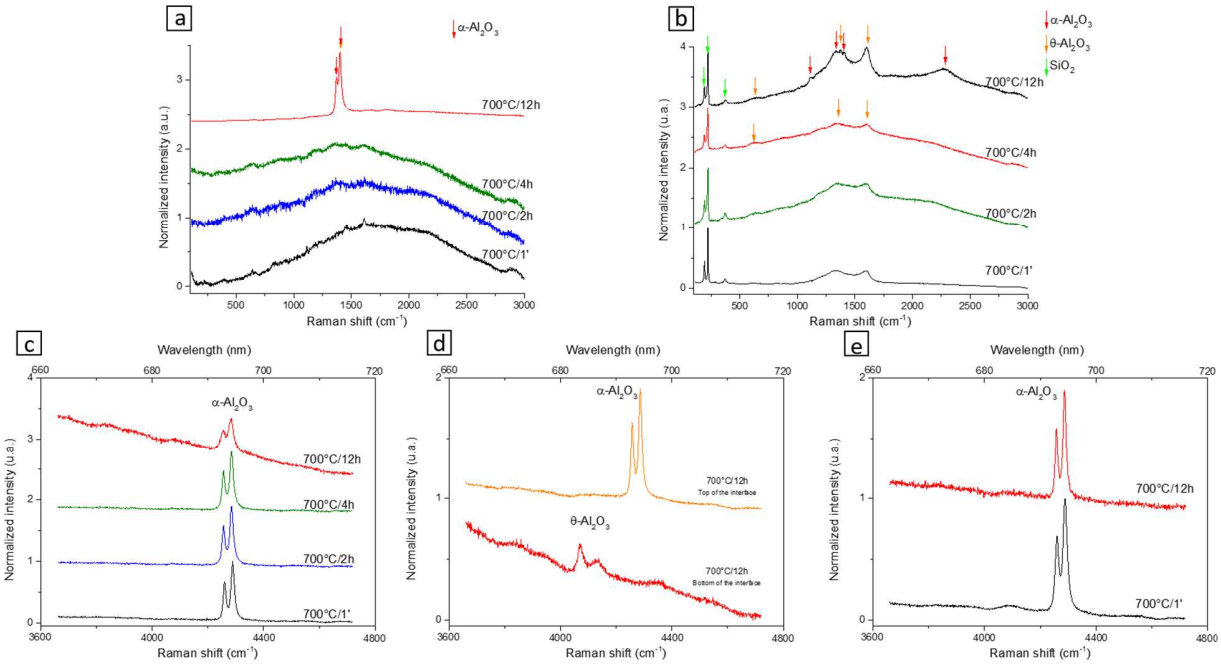

Figure 9: Raman spectra of the particles embedded. (a) and (c) correspond to the particles in the non aluminized layer using λ=632 nm and λ=532 nm, respectively. (b) and (e) are the counterparts in the aluminized layer while (d) is the Raman spectra of the coating/substrate interfacial layer [18-19, 24-25].

3.3. Isothermal oxidation

3.3.1. Aluminizing at 700°C/2h and 1100°C/1min

Figure 10 shows the cross-sections of the coating made after the aluminizing treatment of 700°C/2h (left column) and 1100°C/1 min (right column) on the different substrates. The corresponding EDS concentration profiles are plotted in Figures 11.a & 11.b.

3.3.1.1. Refence coating - Ni raw substrate

Three main layers can be observed in Figures 10.a & 10.b for, respectively, the 700°C/2h and 1100°C/1 min aluminizing treatments. The first layer of about 21±1 µm at the top of the coating consists of many micrometric grains of Al-rich β-NiAl for the treatment of 700°C/2h (Figures 10.a & 11.a), in line with the pioneer work of Pedraza et al. on the slurry aluminizing of pure Ni [8]. In contrast, the grain size obtained with the 1100°C/1 min treatment is similar to the thickness (16±2 µm) of the Ni-rich β-NiAl upper layer (Figures 10.b & 11.b). The second main coating layer is made up of a 2±1 µm thick Ni-rich β-NiAl intermetallic compounds for the 700°C/2h treatment (Figures 10.a & 11.a) and of a 18±1 µm thick layer with a composition close to the Ni_5Al_3 intermetallic compound (Figures 10.b & 11.b) although this phase is supposedly thermodynamically unstable above 700°C [27]. The last sublayers right above the substrate are similar in thickness (~5 µm) (Figure 10) and composition (Ni_3Al) for both coatings (Figures 10.b & 11.b). In addition, one can note the presence of a few round pores in this layer (Figure 10.b).

3.3.1.2. Reference coating – Ni plating

The second reference coating is the diffusion coating obtained on nickel electrodeposits without embedded Al_3Ni_2 micro-reservoirs. The coatings obtained on the Ni plating are made up of several heterogeneous layers (Figure 10.c & 10.d). For the coating of 700°C/2h, the first layer of 31±3 µm consists of Ni-rich β-NiAl intermetallic and displays many defects with a bubble shape escaping from the layer (Figures 10.c & 11.a). Other smaller pores and cracks are also present. In addition, areas with a lower concentration of aluminium (light contrast) can be observed at the bottom of this layer. At the aluminized and non-aluminized layers, a porous interface with aluminium oxide crystals on the edges of the interface appear at higher magnifications (Figure 10.c). The second coating layer seems to correspond to the non-aluminized nickel plating (Figure 10.c). This 21±3 µm thick layer is porous and the aluminium concentration does not exceed 7 at. % (Figure 11.a). Finally, the interface between the coating and the substrate is also porous.

When adding the second aluminizing step of 1100°C/1min, the coating consists of 1 main layer and three very thin layers (Figure 10.d). The first layer is the thickest, with an average thickness of 62±5 µm, and consists of Al-rich β-NiAl as well as pores (Figure 11.b). The pores also take the form of « bubbles » running perpendicular to the surface as if they tried to raise the surface. The three consecutive thin layers towards the substrate are composed of Ni-rich β-NiAl, γ'-Ni_3Al, and γ-Ni(Al). Finally, a porous interface can again be observed between the γ-Ni(Al) layer and the substrate (Figure 10.d).

3.3.1.3. Self-healing coating with "Ni flash"

The coatings studied in this part are composed of first an electrodeposit of pure Ni at 5 A/dm² followed by a second composite Ni+$Al_3Ni_{2(ox)}$ coating at 20 A/dm². For the aluminizing treatment of 700°C/2h, the first layer of 28±2 µm is composed of Ni-rich β-NiAl and pre-oxidized Al_3Ni_2 particles (Figures 10.e & 11.a). In addition, pores vertically aligned appear. The Ni(Al) sublayer corresponding to the Ni electrodeposit has an average thickness of 21±2 µm and ends with an interface containing pores (Figure 10.e). Between the two main coating layers, several very thin layers form but the EDS spot analyses are too large to unambiguously identify any particular intermetallic compound.

Increasing the aluminizing treatment to 1100°C/1 min results in a 34±5 µm thick Ni-rich β-NiAl external sublayer (Figures 10.f & 11.b) over a particle and pore-free zone with a Ni_5Al_3 composition. Below, a porous interface can be observed (Figure 10.f). Next comes the Ni(Al) composite electrodeposit with many pores (Figure 10.f).

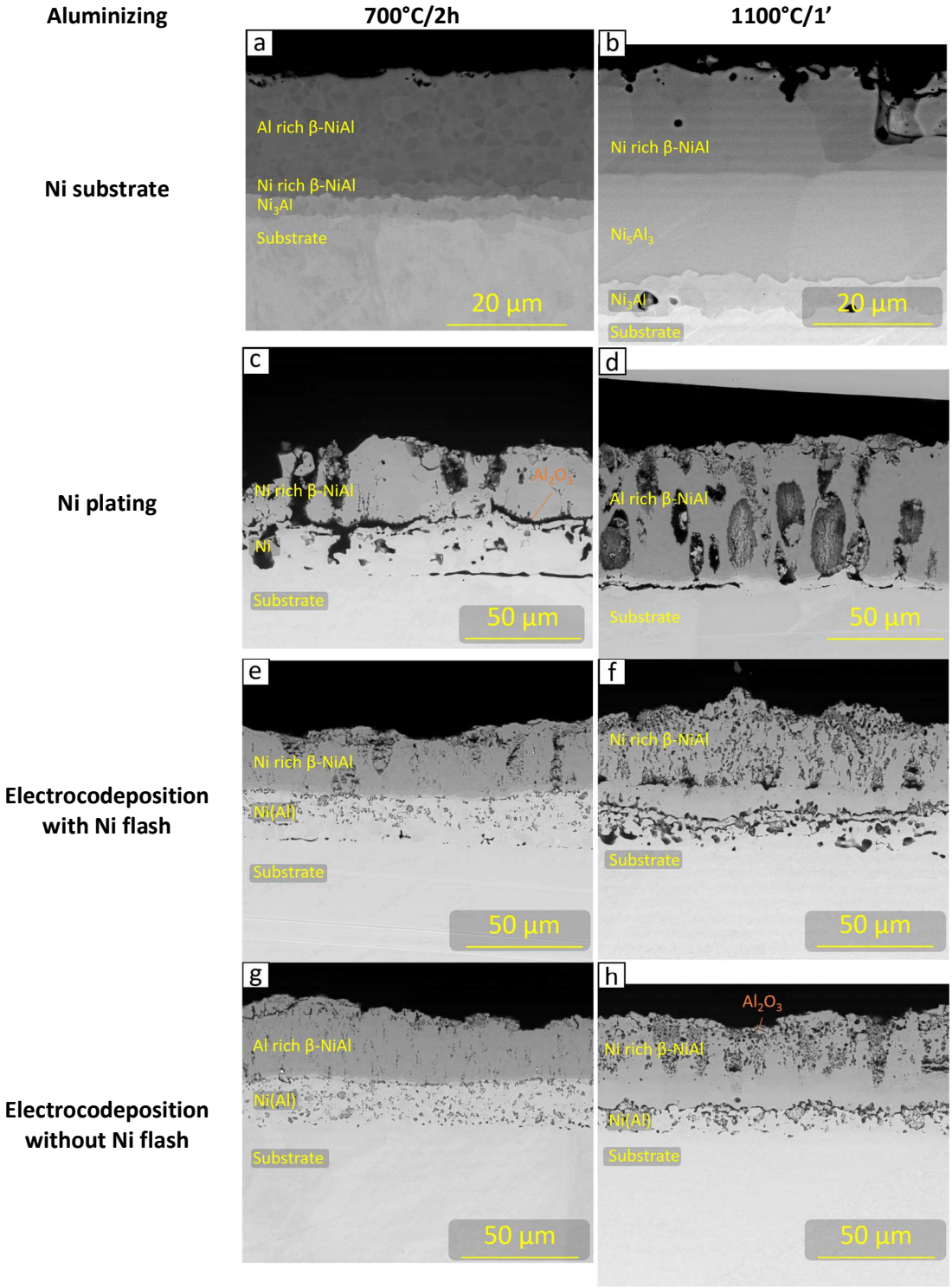

Figure 10: SEM (BSE) cross-section of the aluminized coatings with heat treatment of 700°C/2h and 1100°C/1 min respectively for the Ni substrate (a&b), Ni plating substrate (c&d) and for Ni/Al_3Ni_2(ox) composite electrodeposit with (e&f) and (g&h) without a first layer of Ni.

3.3.1.4. Self-healing coating without "Ni flash"

The last coating studied corresponds to the composite Ni+Al_3Ni_{2ox} electroplating, i.e. without the initial Ni flash electrodeposit. The coatings obtained with an aluminizing heat treatment of 700°C/2h and 1100°C/1min exhibit two distinct zones: a first heavily "aluminized" zone on top of a second "less-aluminized" of Ni(Al) (Figures 10.g & 10.h). The first aluminized layer consists of an Al-rich β-NiAl intermetallic compound for the aluminizing treatment of 700°C/2h (Figure 11.a) while a Ni-rich β-NiAl and Ni_5Al_3 formed when the aluminizing was increased to 1100°C/1min (Figure 11.b). In addition, the Al-rich area contains many pores unlike the Ni-rich area (Figure 10.h). The average thickness of these layers is 29±4 µm and 39±2 µm for respectively, the aluminizing treatments of 700°C/2h and 1100°C/1min. The second layers over the substrate is much less aluminized and Al incorporates into the Ni matrix (substrate) as Ni(Al). It is interesting to remark that the pre-oxidized particles can be readily observed for the 700°C/2h and 1100°C/1min aluminizing treatments (Figures 10.g & 10.h) but the latter also display some pores.

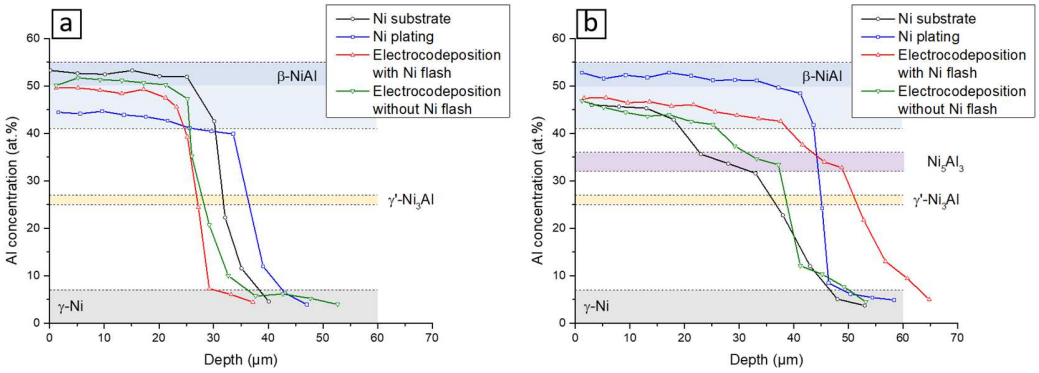

Figure 11: EDS diffusion profiles made in the cross-sections for the different coatings after (a) the aluminizing treatment of 700°C/2h and (b) the isothermal oxidation at 1000°C/48h.

3.3.2. Isothermal oxidation of coatings

Figure 12 shows the cross-sections of the coatings made after the aluminization and isothermal oxidation at 1000°C for 48 in synthetic air. The corresponding EDS concentration profiles of Al are given in Figure 13 while the Raman analyses to identify the oxides that formed after the oxidation treatment are shown in Figures 14 and 15).

3.3.2.1. Refence coating - Ni raw substrate

For the reference coating on the raw substrate, after oxidation at 1000°C for 48h in air, the two main coating layers shown in Figures 12.a & 12.b have the same composition (Ni_5Al_3+Ni_3Al on top and Ni_3Al+Ni(Al) at the bottom, but the thicknesses are slightly greater (30±3 µm and 19±2 µm vs. 13±3 µm and 20±3 µm) with the additional step at 1100°C/1min in line with a fostered interdiffusion. It is also important to note that following the oxidation tests, a thin layer of α-Al_2O_3 developed on the surface of the coatings (Figures 14.a & 15.a). However, for the sake of contrasting conditions in the backscattered electron mode, this 1±0.7 µm oxide layer cannot be observed in Figures 12.a & 12.b

3.3.2.2. Reference coating – Ni plating

For the electrodeposited coating, the aluminide coating becomes surrounded by oxides (Figure 12.c & 12.d). On the surface of the coatings, α-Al_2O_3 with a thickness of 6±2 µm can be observed (Figures 12.c,

12.d, 14.a & 15.a). Below, the composition of the 700°C/2h aluminide coating is that of γ'-Ni_3Al (Figure 12.c) and equivalent to the compound Ni_5Al_3 for the treatment of 1100°C/1min (Figure 15.b). Within the aluminized layer, many grains of α-Al_2O_3 can be observed (Figures 14.b & 15.b). Between the aluminized layer and the non-aluminized layer, a sequence of α-Al_2O_3, $NiAl_2O_4$ and NiO grow following the increasing gradient of Ni towards the electrodeposit (Figures 12.c, 12.d, 14.c & 15.c). In addition, some pores develop in the NiO area of the coatings formed with the addition aluminizing step of 1100°C/1 min (Figure 12.d).

3.3.2.3. Self-healing coating with "Ni flash"

The cross-sections of the two aluminized coatings at 700°C/2h and 1100°C/1' are quite similar with an aluminized layer covered with an α-Al_2O_3 oxide scale (Figures 12.e, 12.f, 14.a & 15.a). The aluminized layer has a composition close to the Ni_5Al_3 compound (Figures 13.a & 13.b) and contains many grains of α-Al_2O_3 (Figure 14.b & 15.b). This layer has an average thickness of 30±10 µm for the heat treatment of 700°C/2h (Figure 13.a) and 19±8 µm for the heat treatment of 1100°C/1min (Figure 12.f). A thin layer of α-Al_2O_3 and $NiAl_2O_4$ spinel (Figure 14.c & 15.c) grows underneath at the interface with the Ni(Al) layer that contains numerous clusters of α-Al_2O_3, spinel NiO and a few pores (Figure 12.f).

3.3.2.4. Self-healing coating without "Ni flash"

For the electro-codeposited coatings, some minor changes occurred (Figures 12.g & 12.h) and relate just to some thickening (34±4 µm) and greater oxidation of the trapped particles to result in Al_2O_3 in a Ni-rich β-NiAl matrix (Figures 13.a & 13.a). The α-Al_2O_3 scale is just 2±1 µm thick and homogeneously covers the coating (Figure 12.g). Another Al_2O_3 oxide layer develops between the Al-rich and the Al-poor layers of the coating, that could act as a diffusion barrier (Figure 14.c). It is also interesting to remark that the $Al_3Ni_{2(ox)}$ particles in the less-aluminized area are oxidized further like in the upper coating layer (Figure 12.g). This suggests that either the coatings are permeable to the external oxygen or that the oxygen of the oxidized particles reacts further to produce more bulky oxides (e.g. $NiAl_2O_4$) or both.

For the samples aluminized at 1100°C/1min, the α-Al_2O_3 present on the top of the coating is thicker than at 700°C/2h because the average thickness is of 12±6 µm (Figures 12.h & 15.a). The layer below has a composition similar to the samples aluminized at 700°C/2h. In addition, numerous oxide particles can be observed in the first part of this layer, which would confirm the above hypothesis, i.e. the coatings would be permeable to oxygen. The potential α-Al_2O_3 diffusion barrier is again observed between the heavily and the poorly aluminized areas (Figure 14.b). One can also note that the grain boundaries of the less-aluminized zone are oxidized (Figure 12.h) forming Al_2O_3 (Figure 15.c).

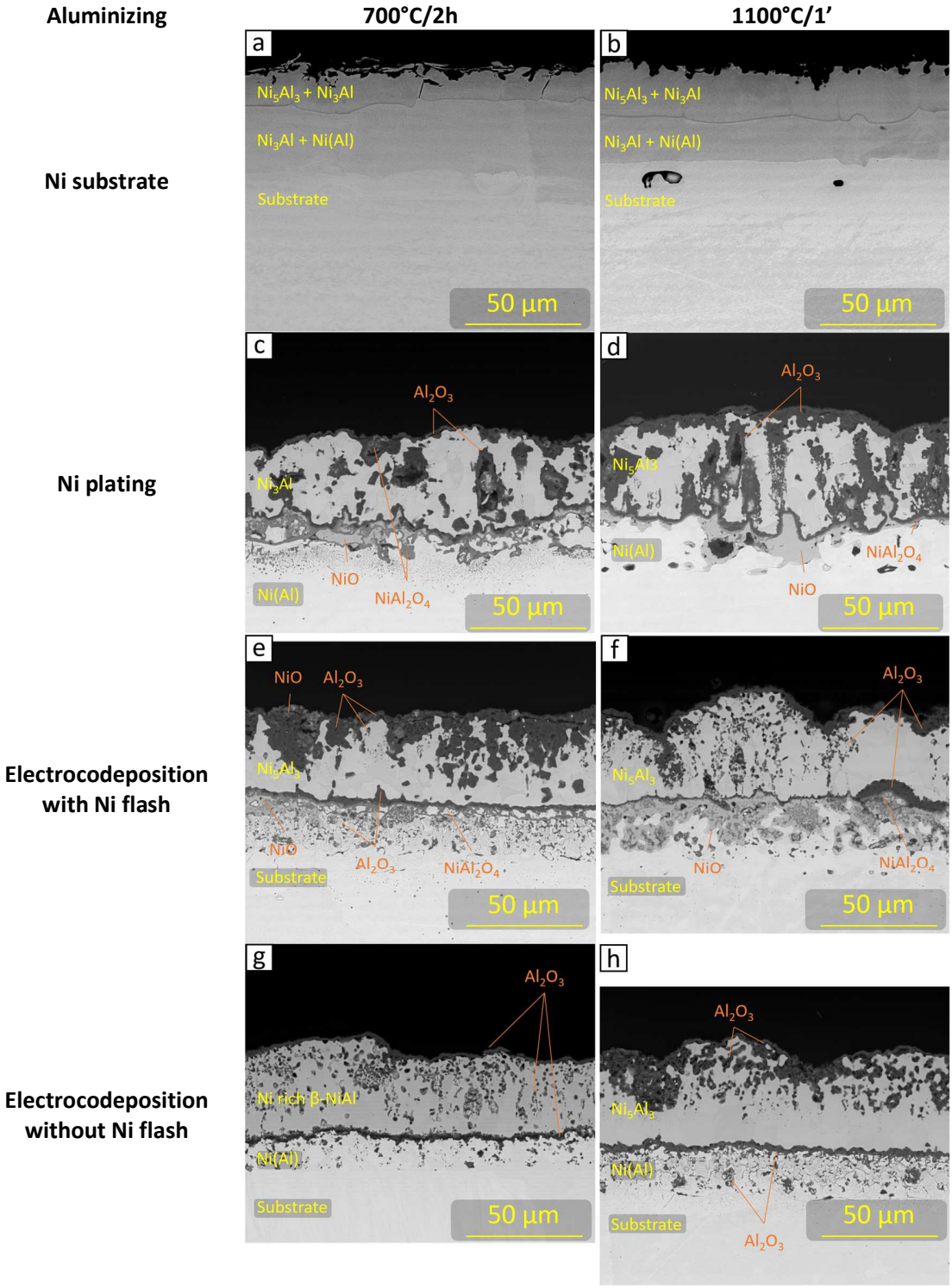

Figure 12: SEM (BSE) cross-section of the aluminized coatings with heat treatment of 700°C/2h and 1100°C/1 min after isothermal oxidation of 1000°C/48h in synthetic air respectively for the Ni (a&b), Ni plating (c&d) and for Ni/$Al_3Ni_{2(ox)}$ composite electrodeposit with (e&f) and (g&h) without a first layer of Ni substrate.

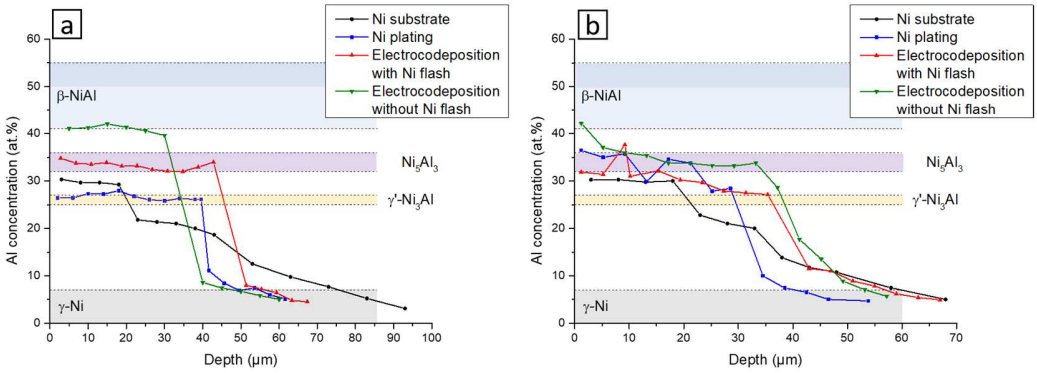

Figure 13: EDS diffusion profiles made in the cross-sections for the different coatings after (a)the aluminizing treatment of 1100°C/1min and (b) the isothermal oxidation at 1000°C/48h.

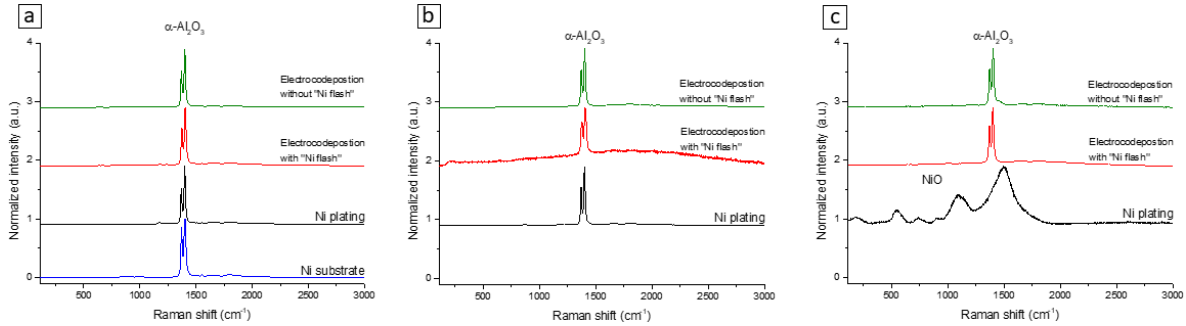

Figure 14: Raman spectra of samples carried out at 700°C/2h after oxidation, with (a) the oxide layer on the surface, (b) the oxide present in the aluminized layer and (c) the oxide present in the less-aluminized layer [18,24].

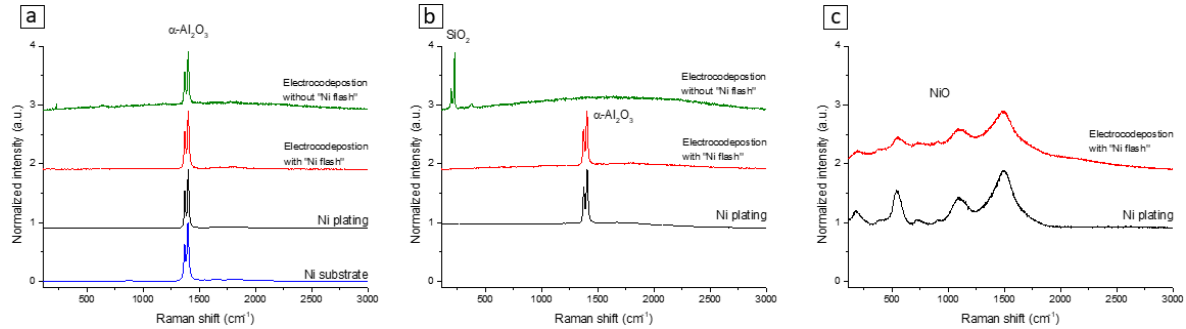

Figure 15: Raman spectra of samples carried out at 1100°C/1min after oxidation, with (a) the oxide layer on the surface, (b) the oxide present in the aluminized layer and (c) the oxide present in the less-aluminized layer [18,24].

.

3.4. Oxidation kinetics

Figure 16 shows the mass gain per surface unit against the isothermal (1000°C) oxidation time (48h) of the different coatings. These curves can be divided into two parts. The first part is characterized by a rapid mass gain, referring to the formation and growth of oxides. The second part is characteristic of a

quasi-stationary regime and characterized by a slow mass gain. During this step, the transformations of the aluminium oxide phase $\gamma \rightarrow \Theta \rightarrow \alpha\text{-}Al_2O_3$ have been proposed by many authors under similar oxidizing conditions [28-29].

For the simple aluminized raw nickel substrates, the mass gains are quite low. These mass gains are less than 0.24 mg/cm² for the aluminized coatings at 700°C/2h and 0.36 mg/cm² for the coatings at 1100°C/1min. These values are in line with other studies on the oxidation of different aluminide coatings on pure Ni [7,21]. For the oxidation of the other coatings with the electrodeposited layers, the mass gains are much greater than for the pure aluminized substrate, in particular when the aluminizing treatment is extended from 700°C/2h to 1100°C/1min as they increase from 3.9 to 6.1 mg/cm².

For the composite electrodeposited coating with the first Ni flash layer, the mass gain is very important for treatment of 700°C/2h with 5.9 mg/cm². For the 1100°C/1min treatment, the mass gain is initially faster but tends to slow down with time to reach 5.6 mg/cm². Without "nickel flash", the mass gains are very close between the two treatments with 2.4 mg/cm². In addition, higher mass gains occur during the first oxidation stages of the 1100°C/1min aluminized samples.

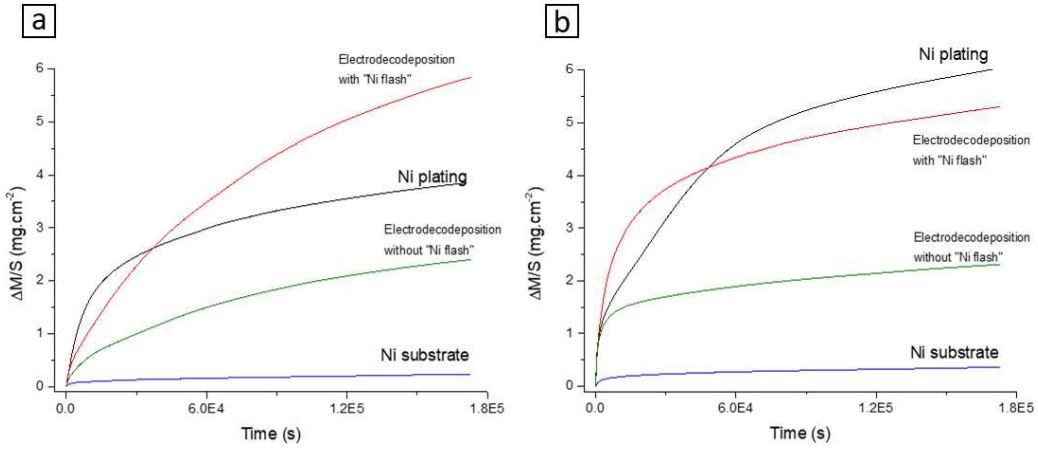

Figure 16: TGA curves of the coatings isothermally oxidized at 1000°C/48h with (a) the coatings aluminized at 700°C/2h and (b) with the extension to 1100°C/1min.

4. Discussion

4.1. Effect of current density on the composite electrodeposit

The electrodeposition conditions (stirring, layout of the electrodes, etc.) make it possible to synthesize a nickel composite electrodeposit with a high concentration of $Al_3Ni_{2(ox)}$ particles. The incorporation of alumina particles into nickel electrodeposits underwent a rapid increase with current density followed by a plateau. The distinctions between the two stages take place around 5A/dm². According to several authors [30-39], the amount of incorporated alumina increases with the decrease of plating current density and increased bath loading. Such authors proposed that increasing the number of effective collisions between the particles and the cathode surface per unit volume of the deposited matrix will increase the amount incorporated into the coating. Therefore, using low current density or high particles concentration in the bath, a large amount of particles can be trapped. However, for an equivalent size and quantity of particles, our results do not agree with such observations but agree with those of Bakhit

et al., who reported a rapid increase in the incorporation of SiC in a nickel/cobalt electrodeposit till 3 A/cm^2 and then the number of embedded particles decreased because in competition with the faster deposition of the metal Ni/Co [40].

A current density of 20 A/dm² was thus selected for the rest of the experiments since it allowed to synthesize a composite electrodeposit containing ~20% vol. particles in a Ni matrix.

4.2. Effect of aluminizing temperature and time

After selecting the parameters and synthesizing the composite electrodeposits, aluminizing by slurry route was carried out to synthesize the self-healing coatings. Various parameters such as aluminizing temperature and time were considered.

The mechanism governing the aluminizing of the substrate at low temperatures is the diffusivity of Al. Indeed, it is accepted that below an aluminizing temperature of 950°C, a High-Activity Low-Temperature aluminizing (HALT) takes place [11,41]. Yet, the mechanisms of slurry aluminizing are somewhat different of the conventional gas phase pack cementation. When the temperatures rise, the aluminium particles of the slurry react with the substrate by solid/solid diffusion and some small diffusion islands start to appear after 600°C/1h [20]. When the temperature reaches 650°C, the self-propagating high temperature (SHS) reactions occur [9], where molten Al dissolves Ni and produces a highly exothermic reaction and the immediate aluminizing of the Ni substrate [8-9]. Therefore, after 1h at 650°C, 35µm of the substrate are already aluminized. This would be in line with the slurry aluminizing mechanisms put down in our research groups a few years ago [8-9,20]. The first step is defined by wetting, dissolution, and formation of a zone of molten aluminium on the surface of the sample. The second step is defined by a majority diffusion of aluminium towards the substrate and a weak diffusion of the nickel towards the aluminium. The intermetallics formed during this step range from the nickel to aluminium-rich phase (γ-Ni→γ'-Ni_3Al→β-NiAl→Al_3Ni_2→Al_3Ni). During this step, an aluminized zone of several tens of microns will form. During the last phase at a higher temperature (T>950°C), the Ni will preferentially diffuse towards the surface to form the desired phase of β-NiAl (Al_3Ni_2→ β-NiAl).

The mechanisms of slurry aluminizing of the electrodeposited coatings at 650°C/12h and 700°C/1min, 2, 4 and 12h are thus similar (Figure 17). Indeed, a first porous layer is formed on the surface. This porous zone is characteristic of a bath of molten aluminium [9]. This molten Al bath will dissolve a thin layer of nickel on the surface and the dissolved nickel will enrich the molten bath (Figure 17.b) [9,20]. For longer aluminizing times, the amount of Al available on the surface will increase (due to the melting of Al particles) and diffusion of Al onto the electrodeposits will quickly occur forming a layer of Al_3Ni_2 intermetallic compound (Figure 17.c), then β-NiAl. This layer will quickly grow until it reaches a thickness of 30 µm. In addition, during this time, nickel will diffuse to the surface and induce the solidification of the molten aluminium bath and the formation of the Al_3Ni and Al_3Ni_2 phases (Figure 17.c). For treatments of 700°C/1min, these different steps have already occurred (Figure 7.a). For longer aluminizing times, a slight thickening of the aluminized zone and a modification of the aluminized/non-aluminized areas interface appears to occur (Figure 7 & 8.a).

In addition, the phases of the aluminium oxide differ between the different layers. In the aluminized areas, the Θ-Al_2O_3 is majorly observed at 650°C and 700°C while the peaks of α-Al_2O_3 are detected after 12h at 700°C for the two laser wavelengths employed in the Raman analyses. In the non-aluminized area, the rapid transformation at low temperature of the Θ → α-Al_2O_3 suggests a low partial pressure of oxygen in this layer, in contrast to the aluminized zone. Networks of defect such as micro-porosities and

trapped gas in the aluminized layer may explain these differences in Po_2. Indeed, part of the trapped gas can be released during the heat treatment and maintain a high Po_2 in the system. This theory seems consistent with the oxidation tests. Indeed, during the oxidation of the two-layers electrodeposited coatings, significant oxidation of the sub-surface of the coating is observed. This internal oxidation could be explained by a network of defects in the aluminized layer. In addition, nickel oxide and spinels form in the non-aluminized layer. According to the Ellingham diagram, the formation of NiO is possible for Po_2 around 10^{-17} and 10^{-11} bar for respectively, 700 and 1000°C. It is therefore probable that the trapped gas in the coating maintains a Po_2 between these two values.

Furthermore, interfacial oxidation occurs around $Al_3Ni_{2(ox)}$ particles (Figure 17.d). The formation of this Al_2O_3 continues all along with the interface. When extending the aluminizing treatment to 12h at 700°C, Kirkendall porosity resulting from the insufficient outward flow of Ni occurs between the coating and the substrate, which provokes interfacial detachment (Figure 17.e). At lower temperature (650°C/12h), no detachment occurs.

For the aluminizing treatment of 1100°C/1min, the first stages of aluminizing are identical. The major differences will occur when the furnace temperature exceeds 950°C. Indeed, at these temperatures, the coating formation mechanisms will go from High to Low-activity (LAHT) following the outward Ni diffusion [11]. Moreover, this diffusion of Ni is clearly observed for the samples aluminized at 1100°C/1min. Indeed, at the bottom of the aluminized layer, a greater Ni concentration and no pores are observed. The lack of pores is caused by the diffusion of Ni which will provide a surplus of atoms allowing gaps and pores to be filled. In addition, at the interface of the aluminized/non-aluminized areas, an interfacial detachment occurs. Finally, at the layers of the first nickel electrodeposit, pores form throughout the thickness of this layer.

For all the aluminizing temperatures, the coatings are porous, and the finer particles appear to dissolve. The porosity of the coating appears to be caused by the nature of the electrodeposits in relation to their fabrication mode. As such, when sufficient thermal energy (e.g. aluminizing temperature) is provided, the defects coalesce and form pores. Regarding the $Al_3Ni_{2(ox)}$ particles, it seems that only the finest particles have been completely dissolved. By comparing the aluminized and the less-aluminized areas of the electrodeposits, the latter contain a large number of particles (Figure 7.a). This clearly implies that, despite the oxide shell exchanges take place between the core of the particles and the external matrix. One may hypothesize that total dissolution of the particles could be prevented by using larger particles or by applying longer pre-oxidation times, hence forming thicker oxide scales.

Overall, the three aluminizing treatments appear to generate quite similar results. Nevertheless, it seems that the treatment of 700°C/12h leads to a lower porosity around the pre-oxidized Al_3Ni_2 particles. An excessive interfacial oxidation can occur during the oxidation step the formation of a thick oxide layer, which would locally decrease the Al content and impede the exchange between the particles and the coatings. For these reasons, a temperature of 700°C was selected for further investigations. For the aluminizing time, the treatment of 700°C/2h was chosen. Indeed, with the extension to 1100°C/1min, a thick residual layer of molten Al bath remains on the surface. For longer times (4 and 12h), cracks appear at the interface that can cause interfacial detachment.

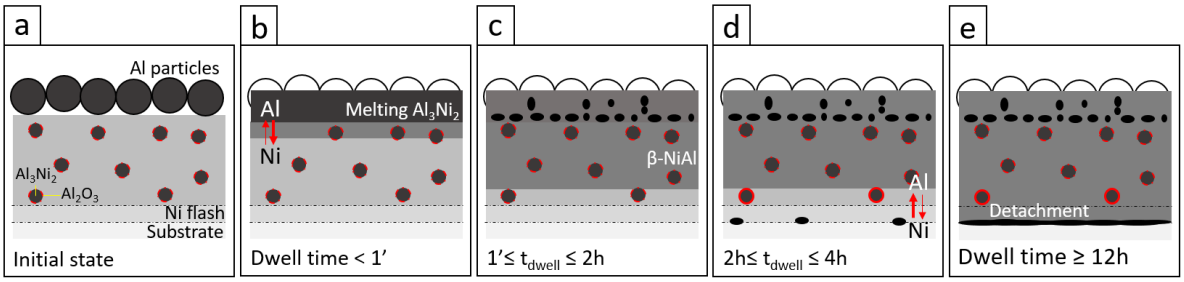

Figure 17: Schematic drawing of the aluminizing process between the composite coating and Al particles heated at 700°C.

4.3. Isothermal oxidation

During this study, preliminary short isothermal oxidation tests (48h) were carried out in air at 1000°C to confirm or refute the self-healing nature of the composite coatings (Figure 18).

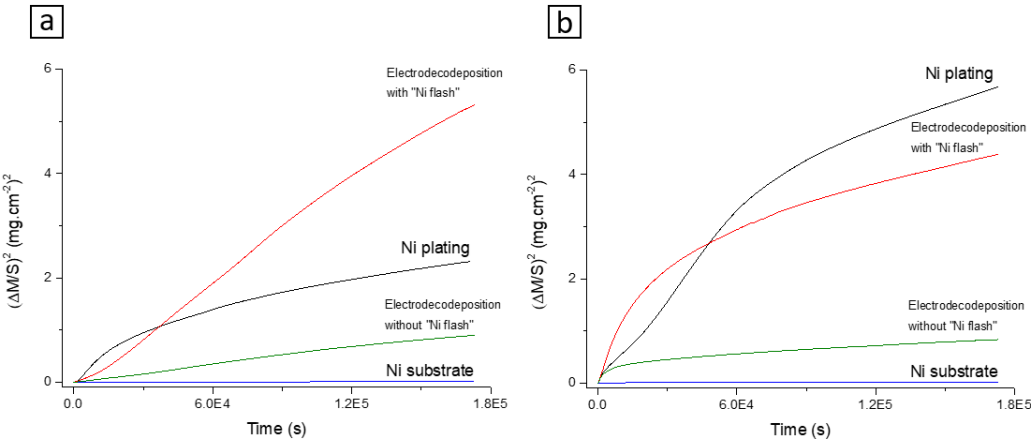

Figure 18: Specific mass variations vs time curves for the aluminized samples for (a) 700°C/2h and (b) 1100°C/1min.

Irrespective of the substrate, the specific mass gain of all the aluminide coatings increases with time of exposure at 1000°C in air and the lowest mass gain is obtained with the aluminized pure Ni substrate (Figure 18). Assuming a parabolic behaviour [42], it appeared that the oxidation of the two aluminizing treatments on the raw substrate result in similar k_p values (Table III). In addition, these values are similar to those obtained for other studies on β-NiAl diffusion coatings elaborated through slurry route (≈2.10^{-9} and 7.10^{-9} $g^2.cm^{-4}.s^{-1}$ for isothermal oxidation at 1000°C) [21,43]. In contrast, the k_p of the aluminized electrodeposits are at least 2 orders of magnitude greater than in the bulk Ni substrate. This greater difference in oxidation kinetics can be explained by three factors, (i) the difference in composition, (ii) the difference in microstructure, and (iii) the presence of internal defects. The microstructure and the composition of the coatings obtained on the Ni electrodeposits are quite similar to those obtained on a raw substrate. Therefore, the main factor that can explain these differences is the presence of defects. Indeed, porosities of several microns are observed in the aluminized layer. In addition, interfacial oxidation and detachment of the oxide scale occur. The formation of spinels and of nickel oxide occurs in the defective areas rather than at the surface of even coatings. As a result, the mass gain is greater and

results in greater k_p values. This clearly implies that the physical meaning of the parabolic rate constant accounting for solid state diffusion cannot really apply to these very uneven situations.

Table III: Parabolic rate constants of the different Al diffusion coatings after 1000°C/48h in air.

Heat treatment	**700°C/2h**	**1100°C/1min**	**Oxidation time**	**48h**	**100h**
Coatings	**k_p ($g^2.cm^{-4}.s^{-1}$)**		**Reference coatings**	**k_p ($g^2.cm^{-4}.s^{-1}$)**	
Ni substrate	$4\ 10^{-8}$	$8\ 10^{-8}$	**Slurry [21]**	$7\ 10^{-9}$	$2.4\ 10^{-12}$
Ni plating	$8\ 10^{-6}$	$2\ 10^{-5}$	**Pack-Cementation [21]**	$8\ 10^{-10}$	$6.1\ 10^{-14}$
Electro-codeposition with "Ni flash"	$3\ 10^{-5}$	$1\ 10^{-5}$	**Slurry [43]**	$2\ 10^{-9}$	$4.7\ 10^{-13}$
Electro-codeposition without "Ni flash"	$5\ 10^{-6}$	$2\ 10^{-6}$			

4.4. Self-healing behaviour

4.4.1. Amount of Al "lost" after the isothermal oxidation

Another method to characterize the high temperature resistance (oxidation and interdiffusion phenomena) of coatings is to calculate the theoretical amount of aluminium in the coatings "lost" during the oxidation. For this, we considered that the coatings extend from the surface of the samples up to a content of 5 Al at.%. Then, the aluminium content (at.%/µm) of the as-deposited coatings and after oxidation is determined with the area under the curve concentration profiles using eq. <1> based on EDS profiles (Figure 11 & 13). All values are gathered in Table IV.

$$[Al] = \int_0^{X(Al_{\%}(X)=5\ at.\%)} Al_{\%}(x)dx$$

With:
x the depth in the coating
$Al_{\%}(x)$ aluminium content at the depth *x (µm)*
X total thickness of the coating (µm)

Eq. <1>

For the reference coatings obtained on the raw substrate, approximately 30 and 20% of the initial quantity of aluminium of the coating were lost by oxidation and by interdiffusion for respectively, the aluminizing treatments of 700°C/2h and 1100°C/1'. In addition, the loss of aluminium is lower for the aluminized coating at 1100°C/1', which suggests a greater stability of the aluminized coating at high temperature against the interdiffusion phenomena.

For the coatings synthesized on the Ni plating, the amount of aluminium lost is high (Table IV). This loss seems to be caused by significant internal oxidation (Figure 12.c & 12.d) due to the numerous cavities present in the coatings after the aluminizing treatment (Figure 10.c & 10.d). In addition, for the Ni plating and on the electro-codeposition with "Ni flash" coatings, the quantity of lost Al is greater for the aluminizing treatments of 1100°C/1'. This difference can be partly explained by the greater amount of defects after the aluminizing step and oxide after the oxidation treatment (interfacial oxidation) (Figure 12.d & 12.f).

Finally, for the electro-codeposited coatings with "Ni flash" aluminized at 700°C/2h and electro-codeposited coatings without "Ni flash", the percentage of aluminium loss is much lower with values between 5 and 10%. Since the oxidation and loss of Al in the reference aluminide coatings is much lower than in the aluminide Al_3Ni_2+Ni composite ones, it derives that the amount of aluminium lost by interdiffusion phenomena in the latter shall be very low and compensate the greater loss of Al by oxidation.

Table IV: Coating thickness and percentage of Al "lost" during the isothermal oxidation (1000°C/48h in air).

Substrate		Coating thickness (µm)	% Al lost
Ni substrate	**700°C/2h**	40	29.4
	1100°C/1'	48	19.2
Ni plating	**700°C/2h**	45	18.4
	1100°C/1'	57	34
Electro-codeposition with Ni flash	**700°C/2h**	36	8
	1100°C/1'	65	25.3
Electro-codeposition without Ni flash	**700°C/2h**	48	5.6
	1100°C/1'	53	6.7

4.4.2. Evolution of the morphology of the coatings

The diffusion coatings obtained on the raw substrate exhibit a similar morphology before and after oxidation. However, the oxidation and interdiffusion phenomena reduce drastically the Al content in the main coating as shown in Figures 11 and 13. As a result, the penetration of Al into the raw Ni substrate is quite significant. For instance, the Al content is of 5 at% at the coating/substrate interface (40 µm) in the as-aluminized substrate but the same concentration occurs at about 95 µm after oxidation for 48h at 1000°C. The gradual depletion of Al will cause several phase transformations that in turn can induce changes in volume and changes in microstructure [27] like the β-NiAl to martensitic $L1_0$ γ'-Ni_3Al with a typical plate-like martensitic microstructure close to the surface. This martensitic structure has been extensively studied and forms when the Al content is around 36-37 at.% [43-48]. Underneath γ'-Ni_3Al, the subsequent layer contains less than 9 at. % leading to the γ-Ni phase with Al dissolved.

On the aluminized nickel electrodeposits, the oxidation induced much greater modifications. This can be attributed to the fact that the coatings contain many defects (pores, cavities, cracks, etc.) after aluminizing. The imprints of bubbles formed during the aluminizing step (Figure 10) could come from trapped foreign species such as hydrogen and/or species coming from the electrodeposition bath. During the aluminizing treatment, the temperature very likely exceeded the value necessary to get gaseous species, which tended to escape from the coating. The defects generated by these "gas pockets" appear smaller close to the surface than those observed deeper in the coating, which could confirm that these gaseous species were indeed able to escape. Deeper in the coating, the "gas pockets" tended to coalesce and to escape but remained trapped in the shape of elongated bubbles. During the oxidation step, these defects play a significant role by facilitating the penetration of oxygen into the coating. As a result,

significant internal oxidation takes place in the coating, with a major formation of α-Al_2O_3 and of NiO at the coating/substrate interface.

The oxidation of aluminized electro-codeposited coatings (Ni flash + composite) is similar than the simple aluminized Ni electrodeposits. Due to the high quantity of defects of the electro-codeposited layer, a thick layer of Al_2O_3 forms on the surface, in the coating and at the interface non-aluminized layer/aluminized layer. In addition, in the non-aluminized layer, a network of aluminium oxide, spinel and nickel oxide are observed. The Al_2O_3 in this layer is probably the one of the pre-oxidized microparticles trapped in this layer. These observations tend to demonstrate that interdiffusion between $Al_3Ni_{2(ox)}$ particles and the nickel matrix takes place.

However, to obtain a functional self-healing coating too many defects are present in the coating. To reduce the presence of defects, it was decided to carry out an oxidation test on composite coatings without the first flash layer of Ni because it oxidizes extremely quickly and introduces many defects that affect oxidation.

The morphology of the aluminized composite coatings without “Ni flash” is quite homogeneous with very few pores and no interfacial detachment compared to the aluminized composites with “Ni flash”. After oxidation, the coating microstructure is quite similar and shows the great metallurgical stability of the coatings, that also maintain a very high concentration of aluminium.

For comparison with the simple aluminide coating made on a raw substrate whose surface aluminium oxide is just about 1 µm thick, the Al_2O_3 scale is barely thicker (2±1 and 12±2 µm respectively for the 700°C/2h and 1100°C/1min aluminizing times). After oxidation, the outermost 20 µm of the simple diffusion coating contain 30 at% of Al while for the self-healing coating the Al content is higher (41 at%) over the entire aluminized area (≈30µm). In this concentration range, the β-NiAl intermetallic compounds are stable. This means that after 48 hours of exposure to 1000°C in air, there is no phase change. Therefore, no change in volume and no internal stresses induced by the phase changes. In addition, a concentration of 5 at. % of Al is observed up to about 94 µm for the simple coatings while for the composite coatings this concentration is reached at 60 µm due to the Al_2O_3 diffusion barrier. The pre-oxidized particles in the non-aluminized area have fully oxidized.

This high concentration of aluminium in the coating appears to be induced by the combined action of the $Al_3Ni_{2(ox)}$ particles and the alumina diffusion barrier. Unfortunately, since the $Al_3Ni_{2(ox)}$ particles are fully oxidized after the oxidation at 1000°C for 48h, it is not possible to quantify the amount of aluminium released by the particles or the effect of the diffusion barrier. Despite this promising result, it appears that the self-healing character of the composite coatings aluminized at 700°C/2h is relatively limited since all of the $Al_3Ni_{2(ox)}$ particles are oxidized, which suggests that the coating matrix is permeable to oxygen.

For the aluminizing treatments of 700°C/2h + 1100°C/1min, the observations are less promising given that a significant portion of the surface of the coatings has oxidized. In addition, strong intergranular oxidation can be observed in the non-aluminized area. This greater oxidation can be caused by a greater diffusion of oxygen through the defect network [49-50]. This network of defects could also explain the greater diffusion of aluminium in the substrate (Figures 11.b & 13.b).

V. Conclusions

The synthesis, pre-oxidation, and incorporation of pre-oxidized Al_3Ni_2 nanometric particles into a nickel matrix by electrodeposition have been investigated in this work. The pre-oxidation treatment of the particles in Ar produced a thin layer of Al_2O_3 on the surface, thus forming particles with an Al_3Ni_2/β-NiAl core and an Al_2O_3 shell. During the electrochemical step and the synthesis of composite coating, the concentration of particles trapped in the coating increased with the current density forming a composite coating containing 20 vol% of pre-oxidized particles homogeneously distributed.

These 50 µm-thick composite coatings were aluminized at 700°C to form a HALT diffusion coating. The coating obtained for an aluminizing treatment of 700°C/2h is made of a first layer of Al-rich β-NiAl (30 µm) and of a second layer of less-aluminized electrodeposit Ni(Al). For longer processing times or higher temperatures, interfacial decohesion occurred, because of the steep composition gradient to the pure nickel substrate

The self-healing nature of the coatings was estimated through isothermal oxidation experiments (1000°C/48h), which turned out quite promising. Indeed, after 48h of oxidation at 1000°C, the aluminium content is of 40 at.% in the first 30 microns of the coating whereas, for a simple diffusion coating, the aluminium content is approximately equal to 30 at.% in the first 20 µm. In addition, only 6% of Al is "lost" by oxidation and interdiffusion compared to the reference coating where about 30% of Al is "lost". This could make it possible, to maintain a sufficient quantity of aluminium to form the protective layer of α-alumina and therefore, to increase the service life of the coating and the protected parts.

Nevertheless, long-term oxidation tests are needed to evaluate the long-term effect on the aluminized composite coating and the alumina diffusion barrier. After 48h of oxidation, the amount of Al has not yet reached critical values. Additionally, cyclic oxidation assays can also be conducted to assess the effect of particles, diffusion barrier, and the delayed β-NiAl → γ'-Ni_3Al transformation.

References

[1]: S.R. White, N.R. Sottos, P. Geubelle, J.S. Moore, M.R. Kessler, S. Sriram, E.N. Brown, S. Viswanathan, Autonomic healing of polymer composites, Nature 409 (2001) 794–7.
https://doi.org/10.1038/35057232

[2]: F. Nozahic, C. Estournes, A.L. Carabet, W.G. Sloff, S. Van Der Zwaag, D. Monceau, Self-healing thermal barrier coating systems fabricated by spark plasma sintering, Materials and Design 143 (2018) 204–213.
https://doi.org/10.1016/j.matdes.2018.02.001

[3]: J.F. Zhao, C. Unuvar, U. Anselmi-Tamburini, Z.A. Munir, Kinetics of current-enhanced dissolution of nickel in liquid aluminium, Acta Materialia 55 (2007) 5592–5600.
https://doi.org/10.1016/j.actamat.2007.06.016

[4]: G.W. Goward, Current research on the surface protection of superalloys for gas turbine engines, JOM 22 (1970) 31–39.
https://doi.org/10.1007/BF03355665

[5]: J. Stringer, High-temperature corrosion of superalloys, Material Science and Technology 3(7) (1987) 482–493.
https://doi.org/10.1080/02670836.1987.11782259

[6]: B.G. Mc Mordie, Oxidation resistance of slurry aluminides on high temperature titanium alloys, Surface and Coating Technology 49 (1991) 18–23.
https://doi.org/10.1016/0257-8972(91)90025-R

[7]: B. Rannou, B. Bouchaud, J. Balmain, G. Bonnet, F. Pedraza, Comparative isothermal oxidation behaviour of new aluminide coatings from slurries coating Al particles and conventional out-of-pack aluminide coatings, Oxidation of Metals 81 (2014) 139–149.
https://doi.org/10.1007/s11085-013-9427-6

[8]: F. Pedraza, M. Mollard, B. Rannou, J. Balmain, B. Bouchaud, G. Bonnet, Potential thermal barrier coating systems from Al microparticles. Mechanisms of coating formation on pure nickel, Materials Chemistry and Physics 134 (2012) 700–705.
https://doi.org/10.1016/j.matchemphys.2012.03.053

[9]: M.C. Galetz, X. Montero, M. Mollard, M. Günthner, F. Pedraza, M. Schütze, The role of combustion synthesis in the formation of slurry aluminization, Intermetallics 44 (2014) 8–17.
https://doi.org/10.1016/j.intermet.2013.08.002

[10]: J.R. Nicholls, Designing oxidation-resistant coatings, JOM 52 (2000) 28–35.
https://doi.org/10.1007/s11837-000-0112-2

[11]: G.W. Goward, D.H. Boone, Mechanisms of formation of diffusion aluminide coatings on nickel-base superalloys, Oxidation of Metals 3 (1971) 475–495.
https://doi.org/10.1007/BF00604047

[12]: E. Perez, T. Patterson, Y. Sohn, Interdiffusion analysis for NiAl versus superalloys diffusion couples, Journal Phase Equilibria and Diffusion, 27(6) (2006) 659–664.
https://doi.org/10.1007/bf02736569

[13]: R. Troncy, G. Bonnet, F. Pedraza, Microstructural characterization of NiAl–Al_2O_3 composite materials obtained by in situ aluminothermic reduction of NiO for potential coating applications, Materials Chemistry and Physics 251 (2020) 123124.
https://doi.org/10.1016/j.matchemphys.2020.123124

[14]: R. Troncy, G. Bonnet, F. Pedraza, Synthesis of self-regenerating NiAl-Al2O3 composite coatings, Materials Chemistry and Physics 279 (2022) 125647.
https://doi.org/10.1016/10.1016/j.matchemphys.2021.125647

[15]: R. Winand, Electrodeposition of metals and alloys-new results and perspectives, Electrochimica Acta 39(8-9) (1994) 1091–1105
https://doi.org/10.1016/0013-4686(94)E0023-S
[16]: B. Bouchaud, B. Rannou, F. Pedraza, Slurry aluminizing mechanisms of Ni-based superalloys incorporating an electrosynthesized ceria diffusion barrier, Materials Chemistry and Physics 143 (2013) 416-424.
https://doi.org/10.1016/j.matchemphys.2013.09.022
[17]: X. Wang, X. Peng, X. Tan, F. Wang, The reactive element effect of ceria particle dispersion on alumina growth: A model based on microstructural observations, Scientific Reports 6 (2016) 29593.
https://doi.org/10.1038/srep29593
[18]: S. Hakkar, S. Achache, F. Sanchette, Z. Mekhalif, N. Kamoun, A. Boumaza, Characterization by Raman spectroscopy of the oxide scales grown on the PM2000 at high-temperatures, Journal of Molecular and Engineering Materials 7 (2019).
https://doi.org/10.1142/S2251237319500035
[19]: A.B. Kulinkin, S.P. Feofilov, R.I. Zakharchenya, Luminescence of impurity 3d and 4f metals ions in different crystalline forms of Al_2O_3, Physics of the Solid State 42 (2000) 857—600.
https://doi.org/10.1134/1.1131301
[20]: G. Bonnet, M. Mollard, B. Rannou, J. Balmain, F. Pedraza, X. Montero, M. Galetz, M. Schütze, Initial aluminizing steps of pure nickel from Al micro-particles, Defect and Diffusion Forum 323-325 (2012) 381–386.
https://doi.org/10.4028/www.scientific.net/ddf.323-325.381
[21]: M. Mollard, B. Rannou, B. Bouchaud, J. Balmain, G. Bonnet, F. Pedraza, Comparative degradation of nickel aluminized by slurry and by pack cementation under isothermal conditions, Corrosion Science 66 (2013) 118–124.
https://doi.org/10.1016/j.corsci.2012.09.009
[22]: F. Pedraza, M. Mollard, B. Rannou, B. Bouchaud, J. Balmain, G. Bonnet, Oxidation resistance of thermal barrier coatings based on hollow alumina particles, Oxidation of Metals 85 (2016) 231–244.
https://doi.org/10.1007/s11085-015-9570-3
[23] X. Montero, M.C. Galetz, M. Schütze, Low activity aluminide coatings for superalloys using a slurry process free of halide activators and chromates, Surface & Coatings Technology 222 (2013) 9–14.
https://doi.org/10.1016/j.surfcoat.2013.01.033
[24]: A.S. Jbara, Z. Othaman, M.A. Saeed, Structural, morphologies and optical investigations of Θ-Al_2O_3 ultrafine powder, Journal of Alloys and Compounds 718 (2017) 1—6.
https://doi.org/10.1016/j.jallcom.2017.05.085
[25]: J. Hruby, S. Vavreckova, L. Masaryk, P. Neugebauer, Deposition of tetracoordinate Co(II) complex with chalcone ligands on graphene, Molecules 25 (2020) 5021.
https://doi.org/10.1063/1.3543838
[26]: D.P. Garriga-Majo, B.A. Shollock, D.S. McPhail, R.J. Chater, J.F. Walker, Novel Strategies for Evaluating the Degradation of Protective Coatings on Superalloys, International Journal of Inorganic Materials 1 (1999) 325–336.
https://doi.org/10.1016/S1466-6049(99)00047-1
[27]: H. Okamoto, Al-Ni (aluminium-nickel), Journal of Phase Equilibria and Diffusion 25 (2004).
https://doi.org/10.1007/s11669-004-0163-0
[28]: M.W. Brumm, H.J. Grabke, The oxidation behaviour of NiAl – I. Phase transformations in the alumina scale during oxidation of NiAl and NiAl-Cr, Alloys Corrosion Science 33 (1992) 1677–1690.
https://doi.org/10.1016/0010-938X(92)90002-K
[29]: K. Shivarni, S. Firouzi, A. Rashidghamat, Microstructures and cyclic oxidation behaviour of Pt-free and low-Pt NiAl coatings on the Ni-base superalloy Rene-80, Corrosion Science 55 (2012) 378–384.

https://doi.org/10.1016/j.corsci.2011.10.037
[30]: K. Barmak, S.W. Banovic, C.M. Petronis, D.F. Susan, A.R. Marder, Structure of electrodeposited graded composite coatings of Ni-Al-Al_2O_3, Journal of Microscopy 185 (1997) 265–274.
https://doi.org/10.1046/j.1365-2818.1997.d01-606.x
[31]: N. Merk, X.M. Ding, B. Ilschner, Detailed microstructural study of electroplated metal matrix composites for gradient hard coatings, Federal Institute of Technology of Lausanne, Switzerland (1994) 377–382.
[32]: V. Greco, W.J.P. Baldauf, Electrodeposition of Ni-Al_2O_3, Ni-TiO_2 and Cr-TiO_2 dispersion hardened alloys, Plating 55 (1968) 250–257.
[33]: M.R. Scanlon, R.R. Oberle, P.C. Searson, R.C. Cammarata, Mechanical properties and deformation behaviour of materials having ultra-fine microstructures, Kluwer Academic Publishers, Boston, MA (1993) 315–321.
[34]: M. Pushpavanam, K. Balakrishnan, L.R. Sharma, Characteristics of Ni-Al_2O_3 electrodeposited composites, Key Engineering Materials 20-28 (1998) 1343–1354.
https://doi.org/10.4028/www.scientific.net/KEM.20-28.1343
[35]: Y.S. Chang, J.Y. Lee, Wear-resistant nickel composite coating from bright nickel baths with suspended very low concentration alumina, Materials Chemistry and Physics 20 (1988) 309–321.
https://doi.org/10.1016/0254-0584(88)90071-5
[36]: M. Verelst, J.P. Bonino, A. Rousset, Electroforming of metal matrix composite: dispersoid grain size dependence of thermostructural and mechanical properties, Materials Science and Engineering: A 135 (1991) 51–57.
https://doi.org/10.1016/0921-5093(91)90536-V
[37]: P.R. Webb, N.L. Robertson, Electrolytic codeposition of Ni-γ Al_2O_3 thin films, Journal of the Electrochemical Society 141 (1994) 669–673.
https://doi.org/10.1149/1.2054789
[38]: F.K. Sautter, Electrodeposition of dispersion-hardened nickel-Al_2O_3 alloys, Journal of the Electrochemical society 110 (1963) 557–560.
https://doi.org/10.1149/1.2425813/meta
[39]: S.W. Banovic, K. Barmak, A.R. Marder, Characterization of single and discretely-stepped electro-composite coating of nickel-alumina, Journal of Materials Science 34 (1993) 3203–3211.
https://doi.org/10.1023/a:100463392368
[40]: B. Bakhit, A. Akbari, Effect of particle size and co-deposition technique on hardness and corrosion properties of Ni-Co/SiC composite coatings, Surface & Coatings Technology 206 (2012) 4964–4975.
https://doi.org/10.1016/j.surfcoat.2012.05.122
[41]: J.M. Brossard, B. Panicaud, J. Balmain, G. Bonnet, Modeling of aluminized coating growth on nickel, Acta Materialia 55 (2007) 6586–6595.
https://doi.org/10.1016/j.actamat.2007.08.025
[42]: B. Pieraggi, Calculations of parabolic reaction rate constants, Oxidation of Metals 27 (1987) 177–185.
https://doi.org/10.1007/BF00667057
[43]: T. Kepa, G. Bonnet, F. Pedraza, Oxidation behaviour of ultrafast slurry aluminized nickel, Surface & Coatings Technology 424 (2021) 127667.
https://doi.org/10.1016/j.surfcoat.2021.127667
[44]: S. Rosen, J.A. Goebel, Crystal structure of nickel-rich nickel aluminium and martensitic nickel aluminium, Transaction of the Metallurgical Society of AIME 242 (1968) 722-4.
[45]: J.L. Smialek, Martensite in NiAl oxidation-resistant coatings, Metallurgical Transactions 2 (1971) 913–915.
https://doi.org/10.1007/BF02662758

[46]: J.L. Smialek, R.F. Hehemann, Transformation temperatures of martensite in β-phase nickel aluminide, Metallurgical Transactions 4 (1973) 1571–1575.
https://doi.org/10.1007/BF02668010
[47]: Y. Zhang, J.A. Haynes, B.A. Pint, I.G. Wright, W.Y. Lee, Martensitic transformation in CVD NiAl and (Ni,Pt)Al bond coatings, Surface and Coatings Technology 163-164 (2003) 19–24.
https://doi.org/10.1016/S0257-8972(02)00585-6
[48]: S.V. Kositsyn, A.I. Valiullin, N.V. Kataeva, I.I Kositsyna, Investigation of microcrystalline NiAl-based alloys with high-temperature thermoelastic martensitic transformation: I. Resistometry of the Ni-Al and Ni-Al-X (X=Co, Si, or Cr) alloys, The Physics of Metals and Metallography 102 (2006) 391–405.
https://doi.org/10.1134/s0031918x06100073
[49]: A.H. Heuer, Oxygen and aluminium diffusion in α-Al_2O_3: How much do we really understand, Journal of the European Ceramic Society 28 (2008) 1495–1507.
https://doi.org/10.1016/j.jeurceramsoc.2007.12.020
[50]: S. Perusin, D. Monceau, E. Andrieu, Investigations of the diffusion of oxygen in nickel at 1000°C by SIMS analysis, Journal of the Electrochemical Society 152 (2005) 390–937.
https://doi.org/10.1149/1.2116787

Electrocodeposition

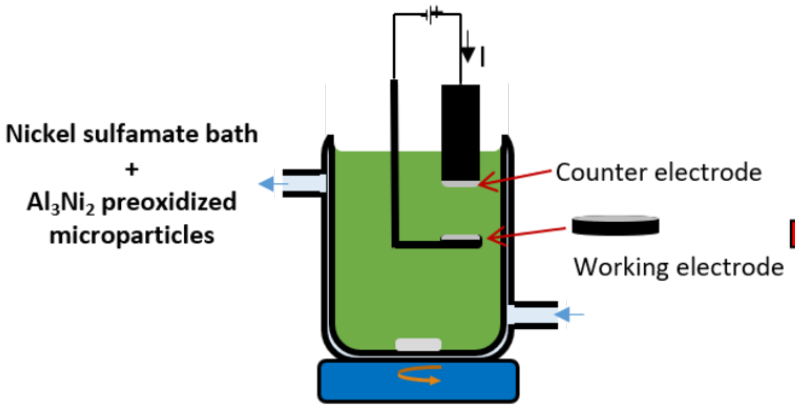

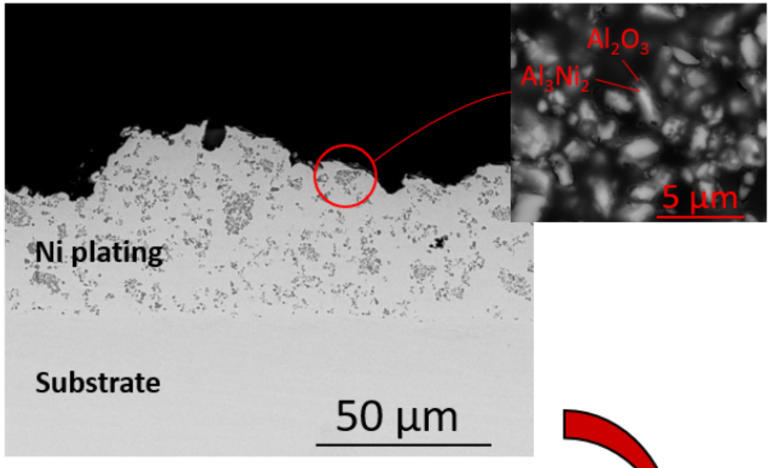

Aluminization heat treatment by slurry way

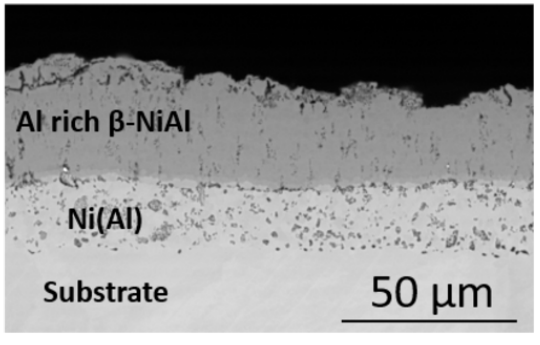

Isothermal oxidation (1000°C/48h)